IEEE Access
Multidisciplinary | Rapid Review | Open Access Journal

Received 24 June 2023, accepted 11 July 2023, date of publication 17 July 2023, date of current version 24 July 2023.

Digital Object Identifier 10.1109/ACCESS.2023.3295993

RESEARCH ARTICLE

Design and SAR Analysis of AMC-Based Fabric Antenna for Body-Centric Communication

USMAN ALI[1], SADIQ ULLAH[1], (Senior Member, IEEE), ABDUL BASIR[2], (Member, IEEE), BABAR KAMAL[3], LADISLAU MATEKOVITS[4,5,6], (Senior Member, IEEE), AND HYOUNGSUK YOO[2], (Senior Member, IEEE)

[1]Department of Telecommunication Engineering, University of Engineering and Technology, Mardan, Mardan 23200, Pakistan
[2]Department of Electronic Engineering, Hanyang University, Seoul 04763, South Korea
[3]Center of Intelligent Acoustics and Immersive Communications, Northwestern Polytechnical University, Xi'an 710072, China
[4]Department of Electronics and Telecommunications, Politecnico di Torino, 10129 Turin, Italy
[5]Istituto di Elettronica e di Ingegneria dell'Informazione e delle Telecomunicazioni, National Research Council of Italy, 10129 Turin, Italy
[6]Department of Measurements and Optical Electronics, Politehnica University Timisoara, 300006 Timisoara, Romania

Corresponding authors: Sadiq Ullah (sadiqullah@uetmardan.edu.pk), Ladislau Matekovits (ladislau.matekovits@polito.it), and Hyoungsuk Yoo (hsyoo@hanyang.ac.kr)

This work was supported by the Institute for Information and Communications Technology Promotion (IITP) Grant funded by the Korean Government, through the Ministry of Science, and Information and Communications Technology and Future Planning (MSIP), under Grant 2022-0-00310.

ABSTRACT This study focused on the design and analysis of an artificial magnetic conductor (AMC)-based fabric antenna for body-centric communication. The antenna was made of felt and had a loss tangent of 0.044 and relative permittivity of 1.3. The proposed antenna was built to function in the frequency band centered at 2.45 GHz, widely used in wireless communication devices. The antenna's performance was evaluated using the electromagnetic simulation software CST MWS. A 50 Ω SubMiniature version connector was used to excite the proposed antenna. A 2 × 2 AMC array was integrated into the antenna below it to improve its performance in terms of radiation efficiency, gain, and backward radiation reduction. The antenna and AMC array were fabricated on flexible fabric substrates. The total volume of the AMC-integrated antenna is $0.55\lambda_o \times 0.55\lambda_o \times 0.016\lambda_o$. It was demonstrated that adding an AMC array enhanced the radiation properties of the antenna and significantly decreased its back lobes. The on- and off-body maximum gains of the AMC-integrated antenna are ($\geq$ 4.11 dBi) and 5.23 dBi, respectively. Furthermore, employing the AMC array, a significant reduction in the specific absorption rate value, which is ($\leq$ 0.43 W/kg) for human body tissue chest/back and ($\leq$ 0.75 W/kg) for human body tissue arm, was obtained, ensuring safety for human use. The simulated and measured results were in agreement. The tested on- and off-body radiation efficiencies in the frequency band centered at 2.45 GHz is (>67%) and (>83%), respectively. The proposed antenna can potentially be used in various applications such as healthcare monitoring, wearable electronics, and Internet of Things (IoT) systems, where reliable and efficient communication is required in a body-centric environment.

INDEX TERMS Artificial magnetic conductor (AMC), body-centric communication, felt, CST MWS, specific absorption rate (SAR), healthcare, IoT.

I. INTRODUCTION

The field of wireless communication has experienced significant growth in recent times, largely driven by the need for more efficient and faster communication systems. Wireless communication has become an essential part of our day-to-day lives, and wearable devices are increasingly popular for various applications such as healthcare, consumer electronics, fitness tracking, military, and entertainment, as they enable wireless communication between wearable

The associate editor coordinating the review of this manuscript and approving it for publication was Santosh Kumar.

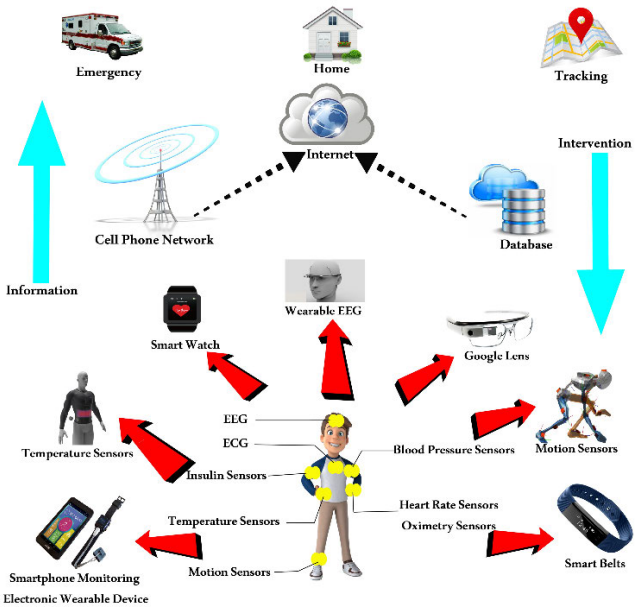

FIGURE 1. Wearable devices and their applications [1], [2].

devices and the surrounding environment, as illustrated in Fig. 1 [1], [2]. In certain specific applications, wearable antennas are the key elements capable of wireless interconnection with adjacent devices, known as body-centric networks, which are related to biological applications [3], [4]. Wearable antenna design is challenging because of its small size, limited bandwidth, high radiation efficiency, and close contact with the human body. Moreover, wearable antennas must be designed with durability, functionality, safety, usability, and convenience in mind [5], [6]. The high conductivity, permittivity, and lossy nature of human body tissue pose significant difficulties in creating an antenna that is efficient, robust, and low-profile when placed close to the body. In addition, electromagnetic radiation can penetrate body tissue, having detrimental effects on one's health. The specific absorption rate (SAR), which quantifies the energy absorbed by tissues when exposed to electromagnetic radiation generated by antennas, is used to compute this effect. Regulatory organizations in numerous countries have determined safe limits for SAR levels. International organizations such as the Institute of Electrical and Electronics Engineers (IEEE) and the International Commission on Non-Ionizing Radiation Protection (ICNIRP) issue recommendations that serve as the foundation for establishing restrictions on the SAR for acceptable human exposure to electromagnetic radiation.

The SAR limits set by regulatory bodies in different countries, such as the United States and the European Union, are based on these recommendations. For instance, the European Union imposed SAR restrictions of 2 W/kg averaged over 10 g of tissue, and the Federal Communications Commission (FCC) set SAR limitations of 1.6 W/kg averaged over 1 g of tissue for cell phones and other similar electronic devices [7], [8], [9], [10].

The following relationship was used to compute the electromagnetic energy absorbed per unit of tissue in the body [11]:

$$\text{SAR} = \frac{\sigma |E|^2}{\rho} [\text{W/Kg}] \tag{1}$$

where, E, σ, and ρ stand for the electric field strength in V/m, the tissue's conductivity in S/m, and tissue density in kg/m^3, respectively.

It is necessary to design antennas integrated into clothing or the human body using flexible textile materials to account for the impact of human movement and posture on their performance. The materials commonly used for this purpose include polydimethylsiloxane, polytetrafluoroethylene, liquid crystal polymers, paper-based substrates, and capton [12]. In addition, textile-based materials such as felt, denim, nylon, wash cotton, fleece, polyester, silk, cordura, jeans, panama, tween, and velcro are growing in popularity because of their flexibility, adaptability, and ease of incorporation into clothing [6]. The radiating element and ground plane of the proposed designs are made of highly conductive textile materials known as e-textiles, such as Shieldit, Zelt, Taffeta, and Flectron, with electrical conductivities of 1.18×10^5 S/m, 1×10^6S/m, 2.5×10^5S/m, and 5.88×10^7S/m, respectively [6].

Body-worn antennas are a rapidly growing research area, particularly in the medical field. Initially, engineers designed wearable antennas to function near the human body; however, the antenna's performance deteriorated in terms of radiation efficiency, gain, and front-to-back ratio. This was because the reflection coefficient (S_{11}) shifted to one side of the resonant frequency depending on the antenna's geometry. Moreover, these antennas were found to emit radiation toward the human body, increasing the SAR threshold values, which could harm the wearer's tissues, as regulated by the governing bodies [13]. Therefore, considering these issues, it is critical to construct wearable antennas with minimal size [14]. Researchers and antenna engineers are actively exploring and developing solutions to these problems.

Many antenna configurations have been designed and described for their suitability as textile antennas, such as planar and vertical monopoles [15], planar waveguides or cavity-backed antennas [16], [17], inverted-F antennas [18], and microstrip patch antennas [19]. However, these antenna designs are large and high profile, offer a narrow bandwidth, have low gain, and produce a high amount of back-lobe radiation, which increases the SAR value. These antennas are unsuitable for body-worn applications for the aforementioned reasons.

Various methods have been proposed to address the challenges faced by wearable antennas [20], [21], [22]. However, these methods have certain limitations. Metamaterials (MMT) have emerged as a potential method to improve the performance of body-worn antennas in body-centric communication. They offer benefits such as stable reflection coefficients, improved functionality, and enhanced

performance, making them ideal for antennas near the human body to transmit and receive signals. MMT is an artificial material with unique electromagnetic properties that can be used to create antennas with superior performance compared with conventional designs [23]. Other alternative MMT designs include the AMC, which imitates the properties of the perfect magnetic conductor (PMC) [24], and the electromagnetic bandgap (EBG), which is used to suppress surface waves [25]. The design of MMT-based wearable antennas involves selecting a suitable metamaterial structure and optimizing it to meet the design requirements such as gain, bandwidth, and efficiency. The MMT structures suggested for wearable antennas include fractal, patch, and planar spiral antennas [26].

Different frequency bands have been reported in the literature, and various studies have been conducted. These bands include the industrial, scientific, and medical (ISM) band, which is centered at 2.45/5.80 GHz [27], [28]; the millimeter wave (mmWave), ranging from 57 to 64 GHz [29], [30], [31], and the ultra-wideband, ranging from 3.1 to 10.6 GHz [32], [33]. However, owing to the availability of a wide range of medical applications, the 2.45 GHz ISM band is suitable and extensively used for body-centric communication.

This study proposed a wearable antenna operating in the ISM frequency range (2.4–2.5 GHz). The substrate for the antenna was made of felt, and it had a loss tangent of 0.044 and a relative permittivity of 1.3. The feasibility of the antenna was initially tested under off-body conditions via simulations and testing. However, a single-band MMT structure was introduced to address the issue of backward radiation toward the human body, which can impact performance and increase the SAR. This structure functioned as an AMC at 2.45 GHz and was integrated into the same fabric-based substrate as the antenna. The proposed designs were then simulated and analyzed on two types of human body tissue models: a flat body model that mimicked the human chest/back and comprised single-, three-, and four-layer models, and a four-layer cylindrical model that mimicked the human arm tissue. CST software was used for the numerical analysis. Finally, the performance of the fabricated prototype was assessed by testing the antenna alone and the AMC integrated into the chest, back, and arms of a volunteer.

The rest of the paper is organized as follows. Section II covers the proposed antenna design and focuses on the design and evaluation of the metamaterial structure. In Section III, the performance of the fabricated prototype is evaluated in both on- and off-body states using both the antenna alone and the AMC-integrated antenna for body-centric communication. Section IV discusses SAR analyses of both designs. Finally, Section V concludes the paper and summarizes the future directions of this study.

II. ANTENNA AND METAMATERIAL DESIGN

The design process for the proposed wearable antenna and the MMT is presented in this section. First, the proposed wearable antenna is designed using a conventional methodology, followed by the design and characterization of the proposed MMT structure in the desired frequency band (2.45 GHz). In the next section, the integration of the MMT structure with the proposed antenna is discussed, and on- and off-body analysis results are presented.

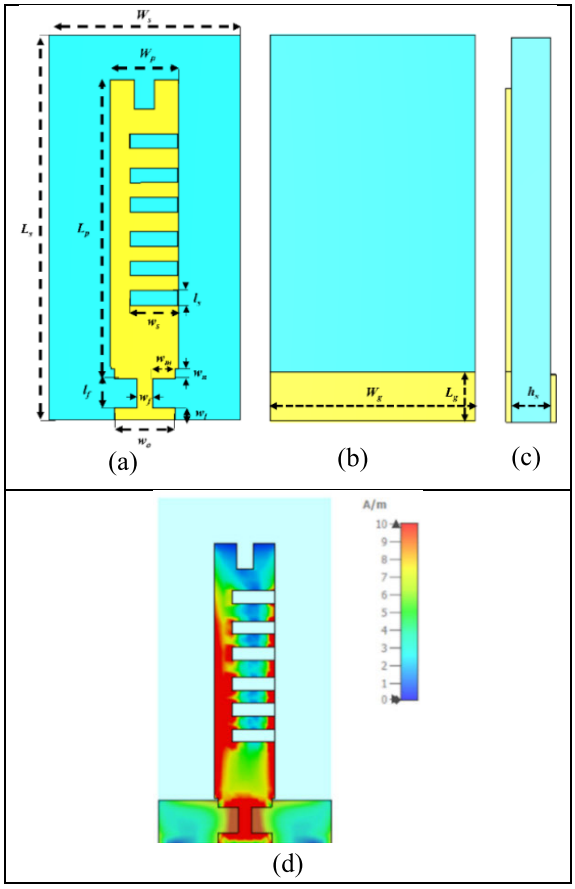

FIGURE 2. Layout of proposed antenna: (a) front view, (b) back view, and (c) side view. (d) Distribution of surface currents.

A. ANTENNA DESIGN METHODOLOGY

The design layout of the proposed wearable antenna, which operates at 2.45 GHz, is shown in Fig. 2. CST Microwave Studio was used to perform the numerical analysis. The substrate used in the proposed design was a felt fabric with a thickness of 2 mm, a relative permittivity of 1.3, and a loss tangent of 0.044. Shieldit, a superconductive material with a thickness of 0.17 mm and an estimated conductivity of 1.85 10^5 S/m, served as the ground plane and radiating components. The total volume of the antenna is $L_s \times W_s \times h_s = 20 \times 40 \times 2$ mm^3, which is equivalent to $0.16\lambda_o \times 0.32\lambda_o \times 0.016\lambda_o$, where λ_o is the wavelength of the free space at 2.45 GHz. The felt fabric was selected based on its availability, low cost, and size range. Table 1 provides a summary of the optimized dimensions of the proposed antenna. An embroidery machine was used to fabricate the antenna, which was then excited using a 50 Ω standard SubMiniature

TABLE 1. Summary of dimensions of proposed wearable antenna.

Parameter	Value (mm)	Parameter	Value (mm)
L_s	40.0	w_o	6.20
W_s	20.0	w_l	1.25
L_p	30.5	w_m	2.30
W_p	7.00	h_s	2.00
l_s	1.50	l_f	3.00
w_s	4.90	w_f	1.60
w_n	1.00		

version A connector. To investigate the antenna performance and current distribution, surface currents were captured at 2.45 GHz, as illustrated in Fig. 2 (d). The currents were largely concentrated along the vertical side, indicating that any adjustment to the radiating element length would affect the antenna's resonance frequency and overall performance. This implies that the length of the radiating element is a significant factor contributing to the antenna's performance.

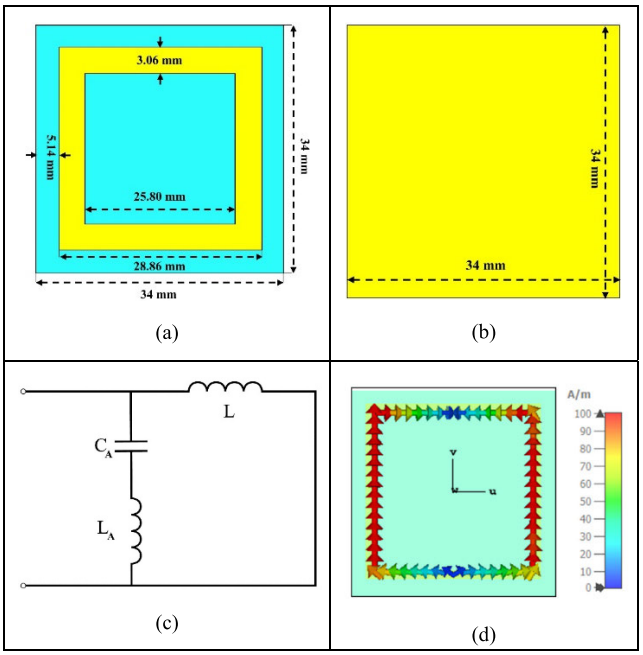

FIGURE 3. Layout of proposed AMC unit cell (a) front view, (b) back view, (c) equivalent circuit, and (d) surface currents distribution.

B. METAMATERIAL DESIGN PROCESS AND CHARACTERIZATION

To ensure safety in body-worn applications, it is vital to stop backward radiation toward the human body while simultaneously enhancing the total performance of the antenna in terms of radiation efficiency, peak gain, and lowering the SAR value. Using MMT to limit the propagation of electromagnetic waves toward the human body is one way of addressing this problem. In this study, an AMC structure was designed, its in-phase reflection was assessed, and its on- and off-body performance was examined when integrated into an antenna. In contrast to the perfect electric conductor (PEC), which has a reflection phase of 180°, the incident wave of the AMC structure has a reflection phase characteristic of 0°. When the antenna is installed on a metal ground plane at a distance of ($<\lambda/4$), the destructive interference of the reflection phase, 180° to the forward radiation, degrades the performance and reduces the total efficiency. However, because of the AMC structure's 0° reflection phase, even at a distance significantly smaller than $\lambda/4$, the original and image currents constructively interfere, resulting in better performance and radiation efficiency. In addition, the AMC surface protects the antenna from body deterioration, maintains stable performance, and limits backward radiation from the human body. Furthermore, the usage of PEC necessitates a substrate with a thickness of ($\geq\lambda/4$) which results in a large antenna size [25].

A simple square-loop AMC is designed, fabricated, and tested. The proposed structure was derived from the conventional Sievenpiper EBG to reduce the conventional dimensions of the unit cell and array of AMC used for integration with the antenna. In addition, a simple structure was chosen because of its ease of customization, fabrication, and low cost. The proposed wearable AMC structure was designed on a 2-mm thick fabric-based substrate, the same as that used in the design of an antenna. A 0.17-mm thick, highly conductive e-textile Shieldit material with a conductivity of 1.18×10^5 S/m was used for the top square loop and ground plane of the proposed AMC structure. The equivalent circuit model of the proposed structure was inspired by [34] and is shown in Fig. 3(c). It is an *LC* series circuit in which the loop metal conductor represents the inductance (L_A), which is calculated using the following relation [34]:

$$L_A = l_n \frac{\mu_o}{4\pi} \ln\left\{1 + \frac{32h_s^2}{w_n^2}\left[1 + \sqrt{1 + \left(\frac{\pi w_n^2}{8h_s^2}\right)^2}\right]\right\}. \quad (2)$$

Because of the gap between the two horizontal conductors of the adjacent unit cells, a capacitance (C_A) is produced and determined by Equation 3 [34], [35].

$$C_A = \frac{W\varepsilon_{0(1+\varepsilon_r)}}{\pi} \cosh^{-1}\left(\frac{W+g}{g}\right). \quad (3)$$

Inductance L_s represents the load and can be determined using the following relation [34] [35]:

$$L_s = \mu_0 h_s. \quad (4)$$

In Equations 2, 3, and 4, μ_o and ε_o denote the permeability and the permittivity of free space, respectively. The gap between neighboring unit cells is represented by g; h_s is the height of the substrate used, and the width of the conductive material of the unit cell is represented by W. The letters l and w represent the length and width of the strip, respectively. The resonant frequency of the proposed AMC can be determined

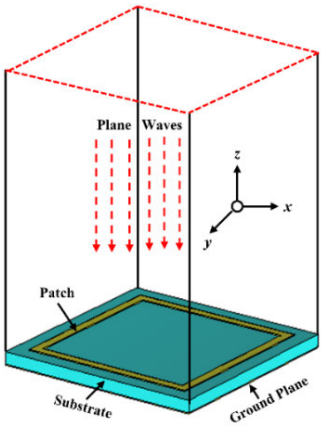

(a)

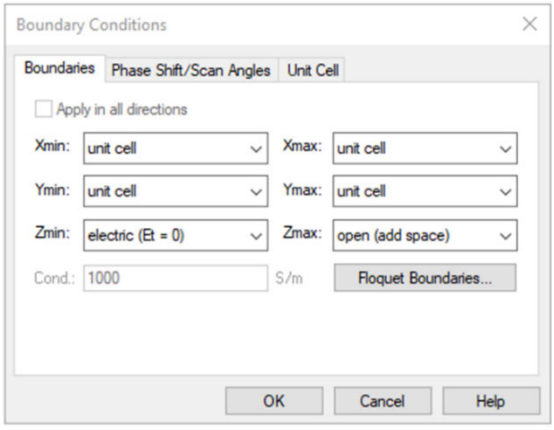

(b)

FIGURE 4. In-phase reflection characteristics simulation setup (a) geometry (b) boundary conditions.

from the inductance and capacitance values using the relationship shown in the following equation:

$$f_r = \frac{1}{2\pi\sqrt{LC}} \tag{5}$$

The total volume of the proposed AMC structure was 34 × 34 × 2 mm^3, which was equal to 0.27 λ_o × 0.27 λ_o × 0.016 λ_o. The dimensions of the AMC unit cell and its optimized arrangement are shown in Fig. 3. For the characterization and numerical analysis of the proposed AMC unit cell, CST MWS simulation software was used to excite the surface with a TE_{10} (linearly polarized) plane wave along the z-axis (from the top, i.e., the negative direction). Fig. 4 depicts the boundary condition and simulation setup for the in-phase characterization of the proposed AMC structure for an incident normal plane wave.

The simulated in-phase response of the proposed AMC structure at 2.45 GHz for a typical incident plane wave is shown in Fig. 5. The bandwidth of the unit cell is 327 MHz (2.4269–2.4596 GHz) between phase values of +90° and -90°, with 2.45 GHz serving as the exact location of the zero-reflection phase. This makes the structure useful as a reflector at resonant frequencies. The reflection phase fluctuates from

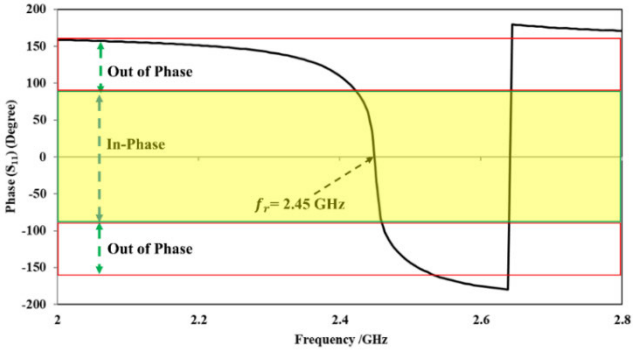

FIGURE 5. Simulated in-phase response of proposed AMC unit cell at 2.45 GHz for normal plane wave incidence.

+180° to +90° and from -90° to +180°, functioning as a PEC. This helps increase the gain, minimize the back lobes of the antenna, and reduce the effects of impedance mismatch caused by lossy human body tissue.

III. RESULTS AND DISCUSSION

This section examines and discusses the on- and off-body performances of the proposed antenna alone and the AMC-integrated antenna.

A. OFF-BODY PERFORMANCE ANALYSIS

This section presents a performance analysis of the proposed antenna alone and AMC-integrated antennas in an off-body situation.

1) ANTENNA IN STAND-ALONE CONFIGURATION

Photographs of the fabricated antenna and measurement setup used to examine the reflection coefficient and far-field radiation patterns at the Applied Bioelectronics Lab at Hanyang University are shown in Figs. 6 and 7, respectively. An Anritsu MS46522A VNA was used to examine the reflection coefficients of the antenna alone and the AMC-integrated antenna in off-body situations, as depicted in Fig. 6(b). Far-field measurements were conducted by placing the antenna in the far-field zone of a broadband horn antenna and mounting it on a positioner.

In Fig. 8, the simulated and measured reflection coefficients of the proposed antenna are presented and compared. The proposed antenna showed a VSWR ≤ 1.2 and an adequate -10 dB bandwidth of 482 MHz at 2.45 GHz in the simulation with a matching of -18 dB. The experimental results validate the effectiveness of the proposed antenna at 2.45 GHz with better -23 dB impedance matching and a -10 dB bandwidth of 610 MHz. Although certain discrepancies may be related to the production and connection processes, the results of the testing and simulations are generally in good agreement, and the ISM band is fully covered.

The far-field gain pattern of the proposed antenna was examined and tested using the measurement setup depicted in Fig. 7. Fig. 9 illustrates a comparison of the simulated

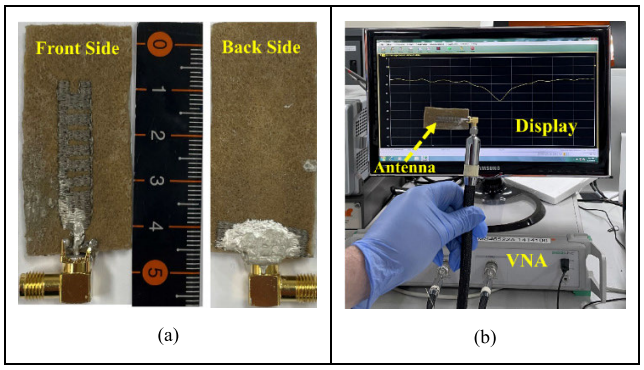

FIGURE 6. (a) Photograph of fabricated prototype of proposed antenna (b) and of measurement setup with antenna under test.

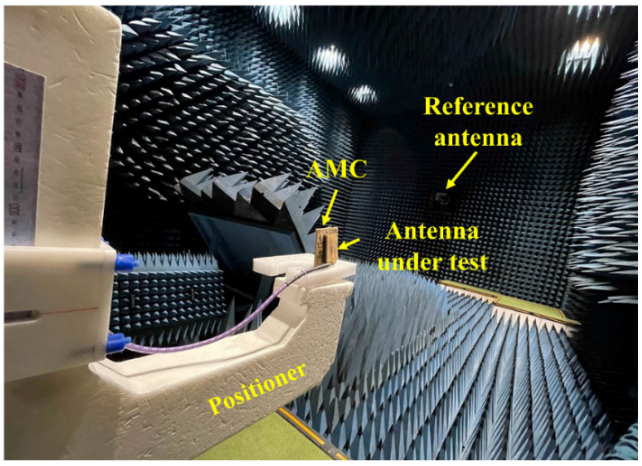

FIGURE 7. Experimentation setup for far-field gain measurement.

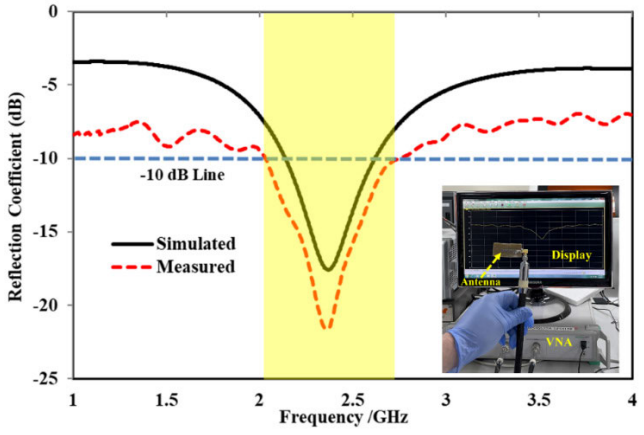

FIGURE 8. Off-body simulated and measured reflection coefficient comparison of proposed antenna alone.

and measured far-field gain patterns. The proposed antenna achieved a maximum gain of 1.26 dBi at 2.45 GHz and displayed a well-known "figure of eight" shape pattern in the E-plane ($\varphi = 90°$) while displaying an omnidirectional pattern in the H-plane ($\varphi = 0°$) pattern. The measured gain was slightly lower than the simulated value; however, the

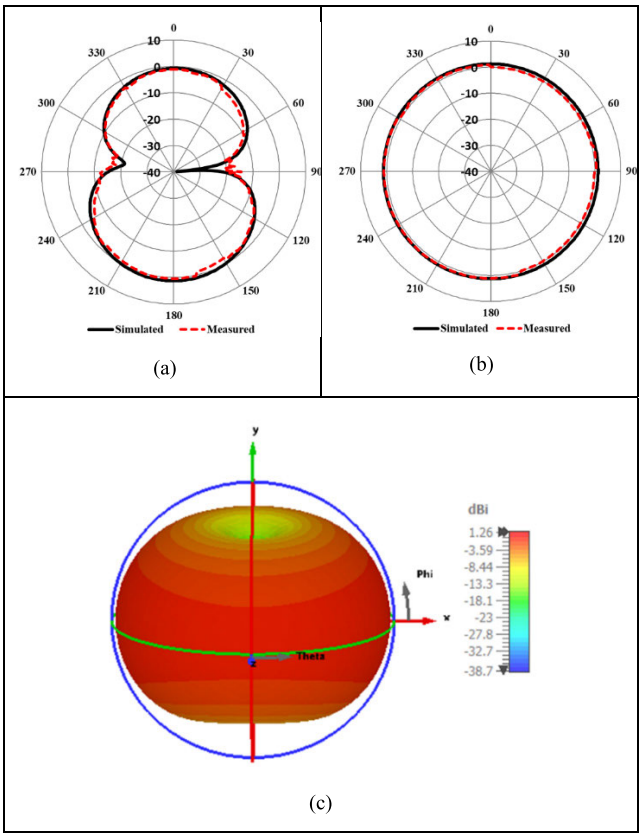

FIGURE 9. Far-field gain comparison of proposed antenna (a) E-plane (b) H-plane (c) 3D pattern.

TABLE 2. Performance comparison of antenna alone.

Parameters	Value @ 2.45 GHz	
	Simulated	Measured
Gain (dBi)	1.26	1.24
VSWR	1.2	1.21
-10 dB Bandwidth (MHz)	418	610
Radiation efficiency (%)	76.20	75.12

difference was negligible, and the antenna maintained its omnidirectional radiation characteristics. This indicates that the fabricated prototype performed similarly to the simulated design, and both the simulated and measured plots exhibited monopole-like radiation, as shown in Fig. 9(a) and (b), respectively. A summary of the simulated and measured performances of the antenna is presented in Table 2. In addition, the 3D gain pattern is shown, confirming that the proposed antenna radiates omnidirectionally (Fig. 9(c)).

2) AMC INTEGRATED ANTENNA

Figs. 10 (a) and (b) depict the arrangements of the integrated design and fabricated prototype, respectively, on the same

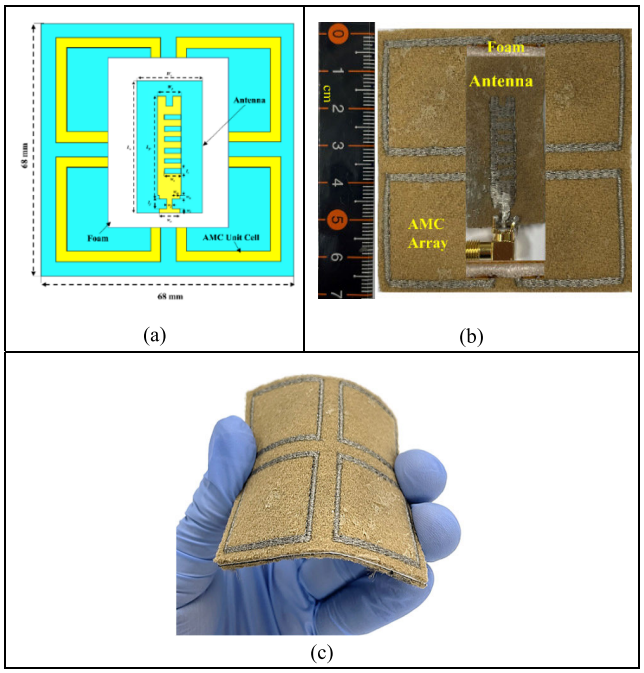

FIGURE 10. Geometry of integrated design of 2 × 2 AMC array (a) CST model, (b) fabricated prototype, and (c) flexibility of material.

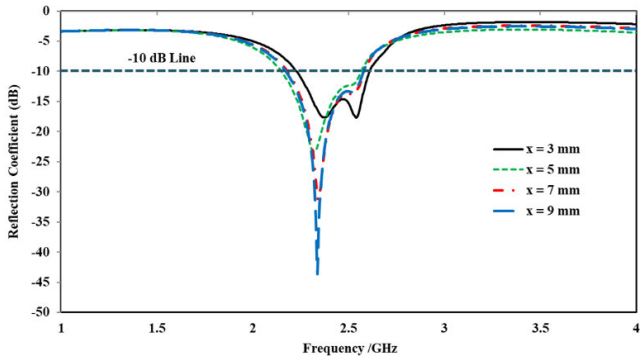

FIGURE 11. Simulated reflection coefficient: comparison for various separations between antenna and AMC plane.

substrate as the antenna. A 2 × 2 MMT structure, which served as the AMC, was placed below the proposed antenna. The configuration comprises three layers: a 2 × 2 AMC array, a Styrofoam material, and the proposed antenna. Commercially available flexible Styrofoam is placed between the antenna and the AMC surface to reduce interaction and avoid short circuits. A 7-mm ($0.05\lambda_o$) thick Styrofoam separation was used in the proposed wearable antenna and 2 × 2 AMC designs to create an integrated structure. A parametric study was conducted by analyzing the antenna's performance at separation distances of 3, 5, 7, and 9 mm to determine the optimal separation distance between the AMC array and the antenna. This study considered the reflection coefficient, gain, and radiation efficiency in free space.

A comparison of the reflection coefficient at various separation distances is shown in Fig. 11. The resonance frequency

TABLE 3. Parametric study with respect to separation between antenna and AMC plane.

Separation (x)	Gain (dBi)	Rad. Efficiency (%)
3 mm	2.03	48.11
5 mm	4.01	66.49
7 mm	5.19	85.73
9 mm	6.23	86.88

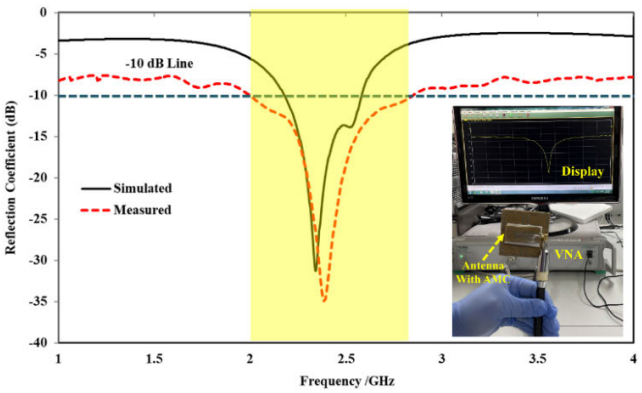

FIGURE 12. Off-body reflection coefficients comparison of AMC integrated antenna at $x = 0.05\lambda_o$.

of the proposed antenna stayed around 2.45 GHz at all separation distances; however, the matching improved as the separation distance increased. The study further observed that the antenna's performance improved with an increase in the separation distance. However, a separation distance higher than 7 mm ($0.05\lambda_o$) increases the total height of the AMC-integrated design. Therefore, a compromise was made between the overall size of the AMC integrated design and the antenna's performance parameters. Hence, a separation distance of 7 mm ($0.05\lambda_o$) was chosen as the optimal distance. A comparison of the peak gain and radiation efficiency for different separation distances is presented in Table 3.

The reflection coefficients comparison of the AMC integrated antenna in the off-body state is presented in Fig. 12, where it is placed above the AMC array at $x = 0.05\lambda_o$. The simulated reflection coefficient reveals a matching of (<-17 dB) at the design frequency (2.45 GHz) with a -10 dB bandwidth ranging from 2.16 to 2.59 GHz. In comparison, the measured reflection coefficient displays a matching of less than -31 dB with a wider -10 dB bandwidth of 810 MHz from 2.05 to 2.86 GHz. However, the simulated and measured results deviated slightly from each other, which could be attributed to factors such as manual fabrication, source errors, or human error. Nevertheless, the proposed AMC-integrated design is appropriate for body-worn applications because it covers the entire ISM band.

The setup shown in Fig. 7 was used to analyze and measure the far-field gain pattern of the AMC-integrated antenna in both principal planes. The antenna alone possesses

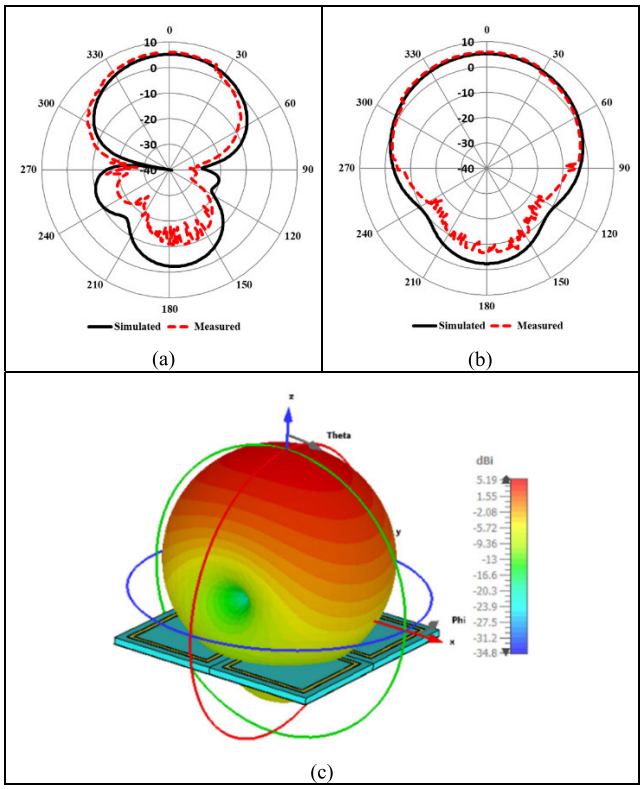

FIGURE 13. Simulated and measured far-field gain comparison of AMC-integrated antenna (a) E-plane, (b) H-plane, and (c) 3D gain pattern.

dipole-like radiation properties in the E-plane ($\varphi = 90°$) and Omni-directional radiation in the H-plane ($\varphi = 0°$), which makes it inappropriate for body-worn applications because it emits unwanted back-lobe radiation toward the body tissue, which is harmful. The simulated and measured gain comparisons of the AMC-integrated antenna in both planes are shown in Fig. 13(a) and (b), respectively. When the antenna is placed above the AMC plane, it converts omnidirectional radiation into directional radiation, enhancing the gain and decreasing the backward radiation, making it suitable for wearable applications. At the design frequency (2.45 GHz), the peak gain of the antenna rises from 1.26 dBi to 5.19 dBi in a direction parallel to the plane of the AMC, demonstrating the advantage of using the AMC as a ground plane. For clarity, Fig. 13 (c) shows the 3D gain pattern of the AMC-integrated antenna at the desired frequency. Owing to the measurement environment, such as connection faults, manufacturing defects, or cable losses, the measured and simulated results were slightly different. A performance comparison between the antenna alone and the AMC-integrated antenna in the off-body state is presented in Table 4.

B. ON-BODY PERFORMANCE ANALYSIS

Antennas, meant to be worn by humans, are designed to function near the human body. However, the lossy and irregularly shaped medium of the human body can negatively affect the antenna's performance, including its radiation pattern,

TABLE 4. Off-body performance comparison of proposed designs.

Parameters	Antenna Alone		AMC-Integrated	
	Simulated	Measured	Simulated	Measured
Gain (dBi)	1.26	1.24	5.19	5.23
Efficiency (%)	76.20	75.12	85.73	83.23
-10 dB Bandwidth (MHz)	418	610	430	810

TABLE 5. Dielectric properties of tissues [6], [10].

Parameters/Tissue	Bone	Muscle	Fat	Skin
Permittivity (ε_r)	18.54	52.72	5.28	38.07
Conductivity (σ) [S/m]	0.81	1.74	0.11	1.46
Loss tangent (tan δ)	0.32	0.24	0.15	0.28
Density (ρ) (Kg/m^3)	1008	1060	911	1109
Thickness (mm)	13.0	20.0	5.00	2.00

resonant frequency, bandwidth, and efficiency [35]. Therefore, when designing antennas, it is important to consider their interactions with the human body. To do this, theoretical and voxel models (sometimes referred to as "phantoms") have been described in the literature [6]. It is vital to evaluate the performance of the proposed antenna close to that of the human body before incorporating it into a wearable system. The proposed and AMC-integrated antennas were simulated and tested on single-and multilayer human body tissues in a wearable work environment. These tissues comprise bone, muscle, fat, and skin layers, and their dielectric properties at the design frequency (2.45 GHz) are listed in Table 5. To simulate the human body tissue, single-layer (homogeneous) and multilayer (nonhomogeneous) tissues were created in flat and cylindrical shapes that represent the chest/back and arm regions of the human body, respectively. Analyzing wearable antennas on different human body models is vital for designing effective and efficient wearable communication systems. The proposed antenna alone and AMC-integrated antenna were analyzed and tested using various human body parts in both flat and cylindrical scenarios.

1) FLAT SCENARIO (HUMAN BODY CHEST/BACK)

This section analyzes the performance of an antenna, both alone and integrated with an AMC, using simplified single-, two-, and three-layer square human tissue models. The sizes of the models for the single and three layers were 180 × 180 × 27 mm^3 and 180 × 180 × 40 mm^3 for the four layers, respectively, which was more than twice the surface area of the intended integrated design. The simulation complexity and associated processing costs were reduced using the reduced model. The proposed antenna was positioned during the simulation at a separation of 1 mm (0.01 λ_o) from the human body tissue to account for the clothing.

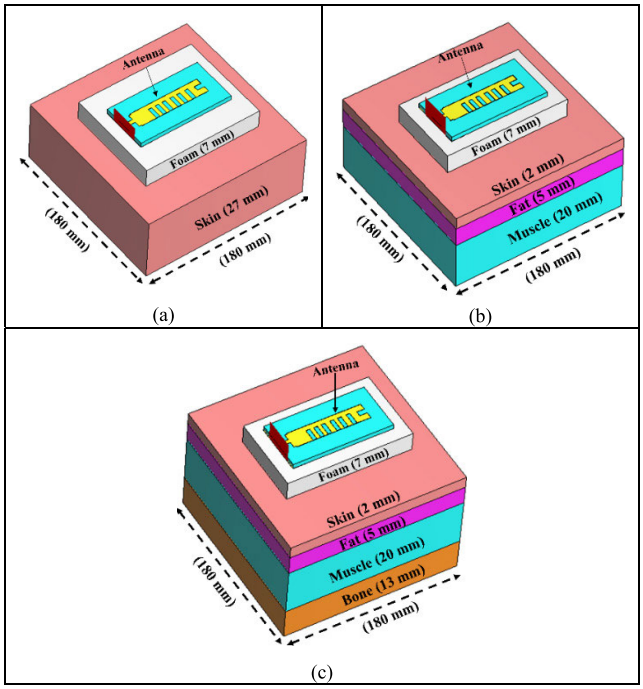

FIGURE 14. Antenna alone mounted on (a) single-layer, (b) three-layer, and (c) four-layer human body models at $x = 0.05\lambda_o$.

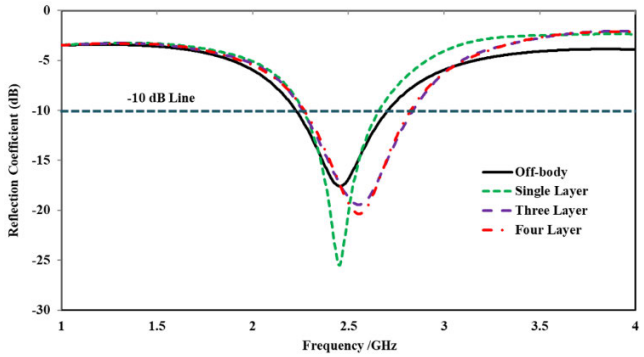

FIGURE 15. On- and off-body simulated reflection coefficients comparison of antenna alone when positioned on numerous layers of flat body phantom (chest/back) at $x = 0.05\lambda_o$.

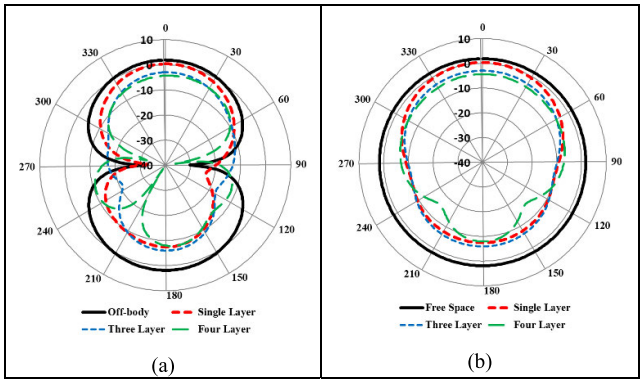

FIGURE 16. On- and off-body simulated gain comparison of proposed antenna alone in (a) E-plane (b) H-plane at $x = 0.05\lambda_o$.

Subsequently, a performance analysis of the proposed designs for various layered models in terms of peak gain, reflection coefficient, impedance bandwidth, and radiation efficiency was performed.

a: ANTENNA ALONE

Various layered models have varying effects on antenna performance. Single-layer models, for instance, have a less significant impact than multilayer models. As shown in Fig. 14 (a), the body tissue behaved more like a homogeneous medium with a single set of dielectric properties when the antenna was positioned on a single-layer model at $x = 7$ mm ($0.05\lambda_o$). In this case, the signal only passes through a single layer with generally consistent dielectric characteristics, reducing the effect of human body tissue on the antenna's performance. However, the high dielectric constant of the skin layer compared to that of air can lead to a shorter electrical length for the antenna, which can cause the antenna to radiate less efficiently and direct less energy in the desired direction.

Consequently, the antenna's peak gain, radiation efficiency, and impedance were affected. However, this effect was less significant than that in the multilayer model. When the antenna was placed on a three-layer model of human tissues, such as muscle, fat, and skin, at $x = 7$ mm ($0.05\lambda_o$) (Fig. 14(b)), the signal passed through these three layers, each with its specific electrical properties, including permittivity and conductivity, which can cause signal attenuation and distortion, resulting in a significant reduction in peak gain and radiation efficiency. In addition, as the antenna's electrical length decreased owing to variations in the dielectric constants of each layer, the resonance frequency detuned to the right, as shown in Fig. 15. When the antenna is mounted on a four-layer model at $x = 7$ mm ($0.05\lambda_o$), as shown in Fig. 14 (c), which includes an additional layer of bone, the signal must pass through an additional layer of tissue with a higher permittivity and conductivity.

In addition, bone has a high electrical impedance compared with soft tissue. As a result, the signal passing through the bone experiences significant attenuation and phase shift. Consequently, the antenna's radiation efficiency and peak gain were severely affected. In addition, the resonance frequency detunes to the right because of the change in the dielectric constant (Fig. 15). This leads to the conclusion that compared to a single- or three-layer model, a four-layer model of human tissue has a higher impact on the antenna peak gain and radiation efficiency.

Figs. 15 and 16 show the on- and off-body simulated reflection coefficients and gain comparison, respectively, of the antenna mounted on the single-layer, two-layer, and three-layer models at $x = 7$ mm ($0.05\lambda_o$). For clarity, snapshots of the 3D gain patterns for various layers are shown in Fig. 17.

b: AMC-INTEGRATED ANTENNA

As previously discussed, phantoms that approximated single, three, and four layers of human body tissue were used to analyze the performance of the AMC-integrated antenna

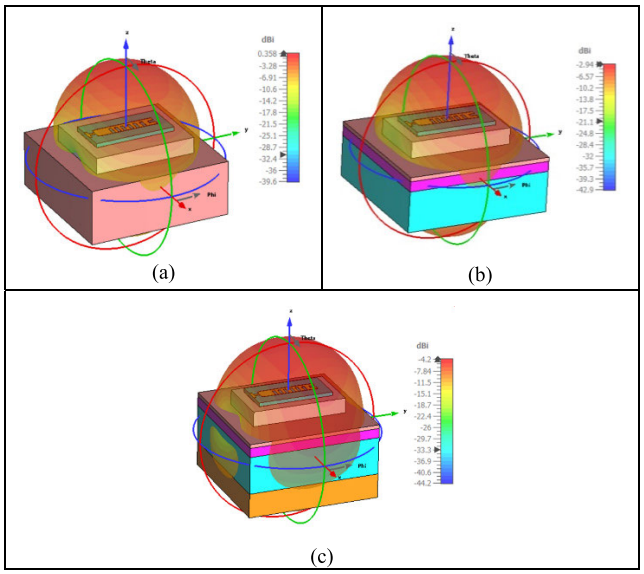

FIGURE 17. Simulated on-body 3D gain pattern of antenna alone for given frequency on (a) single-layer, (b) three-layer, and (c) four-layer flat body phantom (chest/back) at $x = 0.05\lambda_o$.

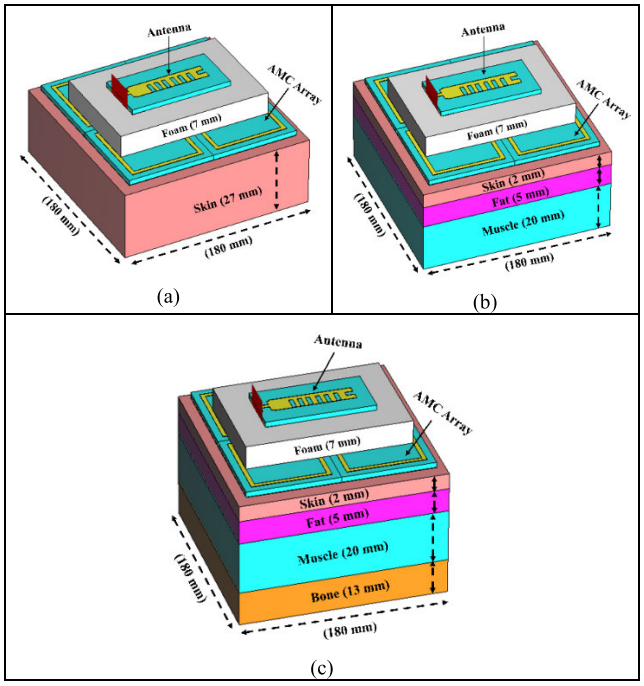

FIGURE 18. AMC-integrated antenna mounted on (a) single-layer, (b) three-layer, and (c) four-layer human body models.

(Fig. 18). The AMC was positioned 1 mm (0.01 λ_o) above the human-body tissue model. This separation represents cloth thickness in real-world situations. The antenna was maintained at a distance of $x = 7$ mm ($0.05\lambda_o$) from the AMC plane.

The primary goal of integrating the AMC surface into the antenna design is to protect it from harmful impacts on the body, which can impair the antenna's performance. In addition, employing the AMC as a reflector with an antenna on a

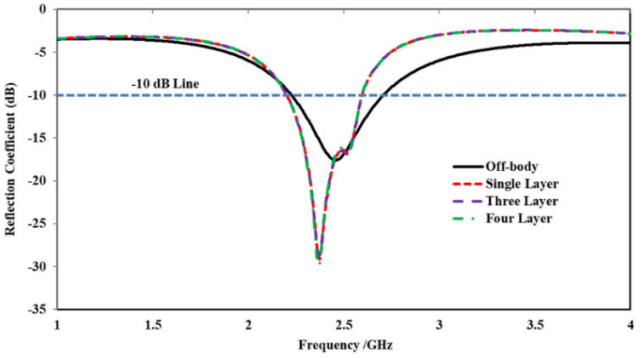

FIGURE 19. Simulated on- and off-body reflection coefficient comparison of AMC-integrated antenna on flat body phantom (chest/back) at $x = 0.05\lambda_o$.

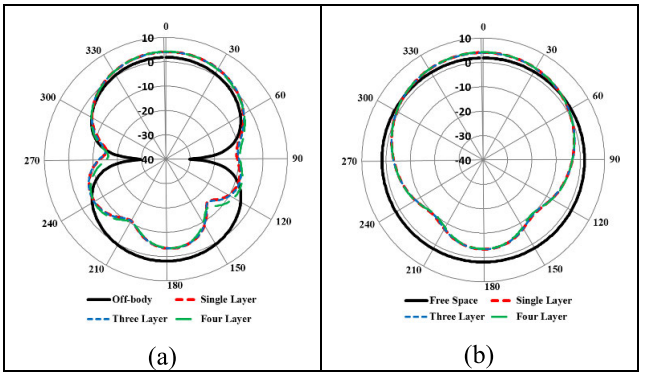

FIGURE 20. Simulated on- and off-body gain comparison of AMC-integrated antenna in (a) E-plane and (b) H-plane at $x = 0.05\lambda_o$.

human body phantom can enhance the antenna's performance by minimizing the phantom's influence on the antenna. The AMC ground plane reduces the amount of energy absorbed by the phantom, thereby reducing the coupling between the antenna and phantom, increasing the efficiency and impedance bandwidth of the antenna, and boosting impedance matching. Fig. 19 illustrates the simulated reflection coefficient, which indicates that the AMC-integrated antenna exhibited a stable response regardless of the tissue layer and provided a peak gain of more than 4 dBi in both principal planes (Fig. 20). For further clarity, a perspective view of the 3D simulated gain pattern is included (Fig. 21). Table 6 compares the simulated performances of the proposed antenna designs on different tissue layers in terms of peak gain, radiation efficiency, resonance frequency, and impedance bandwidth.

The performances of the fabricated prototype designs of both the antenna alone and AMC-integrated antenna were tested in a real-world scenario by employing them on the chest and back of a male volunteer, as shown in Fig. 22. As previously explained, the four-layer human body tissue significantly impacts the antenna's overall performance. Consequently, the on-body performance analysis of the prototype design and simulation results obtained by mounting

TABLE 6. Summary of simulated performance comparison on various tissue layers.

Tissue Model	Antenna Alone				AMC-Integrated			
	Frequency (GHz)	Gain (dBi)	Rad. Eff. (%)	BW (MHz)	Frequency (GHz)	Gain (dBi)	Rad. Eff. (%)	BW (MHz)
Single-Layer	2.45	0.36	22.65	400	2.43	4.13	72.89	410
Three-Layer	2.55	-2.94	15.11	556	2.44	4.05	71.06	405
Four-Layer	2.56	-4.20	13.42	578	2.44	4.21	73.82	405

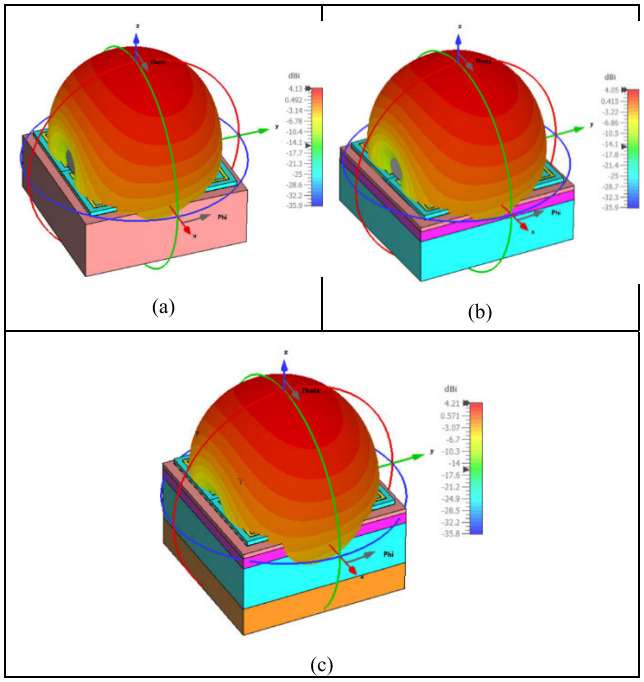

FIGURE 21. Simulated on-body 3D gain pattern of AMC-integrated antenna at 2.45 GHz on (a) single-layer, (b) three-layer, and (c) four-layer flat body phantom (chest/back).

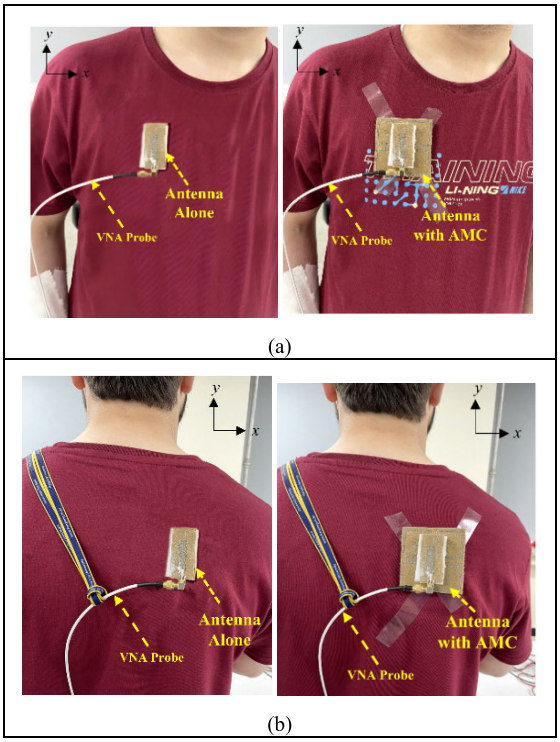

FIGURE 22. Proposed antenna alone and AMC-integrated antenna mounted on body of volunteer (a) chest (b) back.

the antenna on a four-layer human body tissue model were compared.

The on-body reflection coefficients of both the antenna alone and the AMC-integrated antenna were tested. The results were compared with those obtained by simulating the antenna placed on four-layer human body tissue (Fig. 23). The resonance frequency shifts to the right when the antenna is positioned on the back or chest of the human body, as indicated by the dotted blue line in Fig. 23. Conversely, the AMC-integrated antenna exhibited improved impedance matching (S_{11} < -35 dB) when placed on the back or chest of the human body, and the desired resonance frequency at 2.45 GHz was also maintained. In addition, in both cases (antenna alone and AMC-integrated), a broader -10 dB bandwidth of 850 MHz (1.96–2.81 GHz) was obtained, which is attributed to the additional losses caused by the human body proximity [34]. The simulated and test results were in good agreement, demonstrating the potential of the proposed AMC-integrated antenna for body-worn applications.

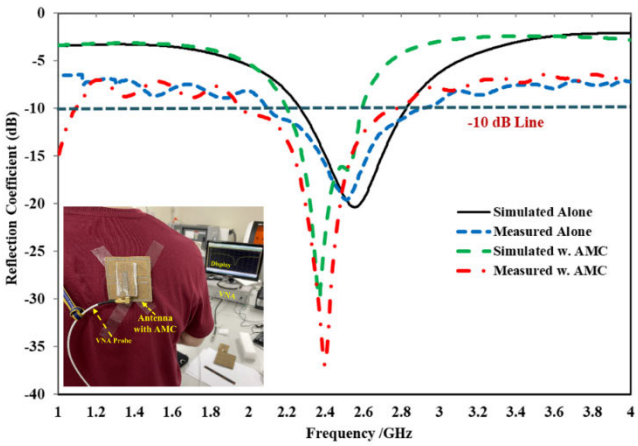

FIGURE 23. On-body simulated and measured reflection coefficient comparison of antenna alone and AMC-integrated antenna at x = 0.05λ_o on flat body section (chest/back) of volunteer.

The gain patterns of the proposed antenna alone and AMC-integrated antenna were measured at 2.45 GHz using the measurement setup depicted in Fig. 7. The designs were tested at two different locations on the volunteer's chest and back, and the gain was measured in both principal planes.

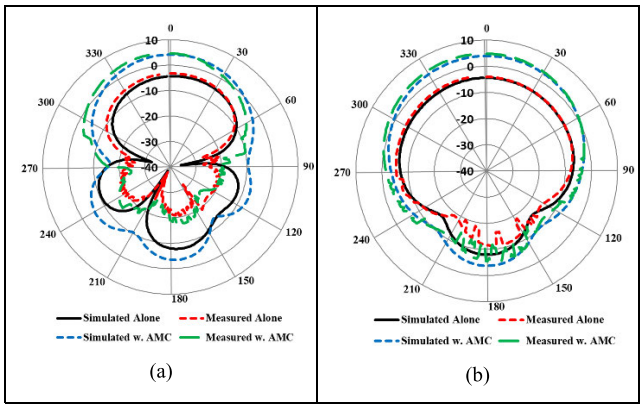

FIGURE 24. On-body simulated and measured radiation pattern gain comparison of antenna alone and AMC-integrated antenna in (a) E-plane (b) H-plane.

TABLE 7. On-body performance comparison of proposed designs mounted on human chest/back.

Parameters	Antenna Alone		AMC-Integrated	
	Simulated	Measured	Simulated	Measured
Frequency (GHz)	2.56	2.53	2.44	2.46
Gain (dBi)	-4.20	-3.92	4.21	4.62
Rad. Eff. (%)	13.42	14.55	73.82	75.77
BW (MHz)	578	620	405	850

The measured results were compared with the on-body simulation results obtained from the four-layer simplified tissue model, as depicted in Fig. 24. The radiation pattern of the antenna deteriorated when it was in close proximity to the human body, which dramatically decreased its peak gain and radiation efficiency. However, the on-body peak gain and radiation efficiency increased significantly when the AMC-integrated antenna was tested at the same two positions, demonstrating the advantages of using the AMC as a ground plane. The measured far-field on-body gain was slightly lower than the simulated gain. Table 7 provides a summary of the on-body performance comparison between the proposed antenna alone and AMC-integrated antenna.

c: CYLINDRICAL SCENARIO (HUMAN BODY ARM)

In this section, a human tissue model comprising four layers that resemble the human arm is used to examine the performance of the proposed antenna alone and AMC-integrated antenna. The arm model has a length and overall radius of 180 and 40 mm, respectively, which correspond to the arm radius of a healthy man, as illustrated in Figs. 25 (b) and (c). The four layers comprised bone, muscle, fat, and skin were modeled in CST MWS using the intrinsic characteristics of each layer using the data in Table 5. Subsequently, the proposed designs were tested by employing them on a real human arm, as shown in Figs. 25 (d) and (e). Fig. 26 shows a comparison of the simulated and measured reflection coefficients of the proposed designs mounted on a four-layer human arm. The results revealed that placing the antenna

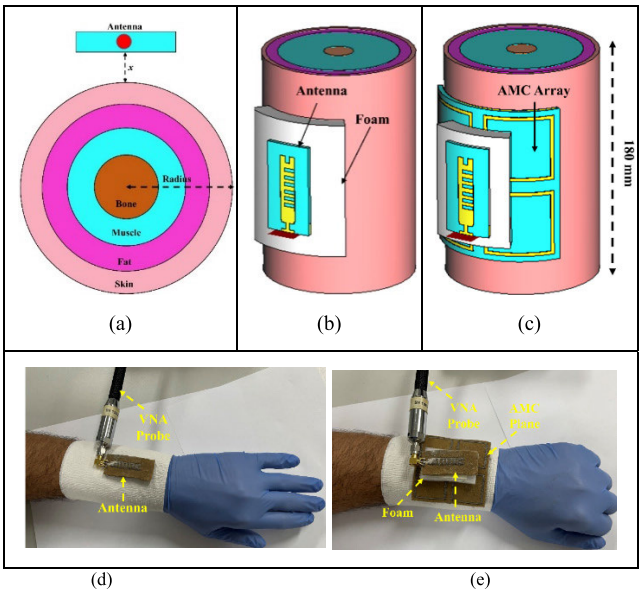

FIGURE 25. Layout of proposed antenna mounted on four-layer cylindrical phantom (human body arm) of radius, r = 40 mm (a) top view of layered structure (b) CST model of antenna alone (c) CST model of AMC-integrated antenna (d) fabricated antenna alone (e) fabricated AMC-integrated antenna mounted on human body arm at x = 0.05λ_o.

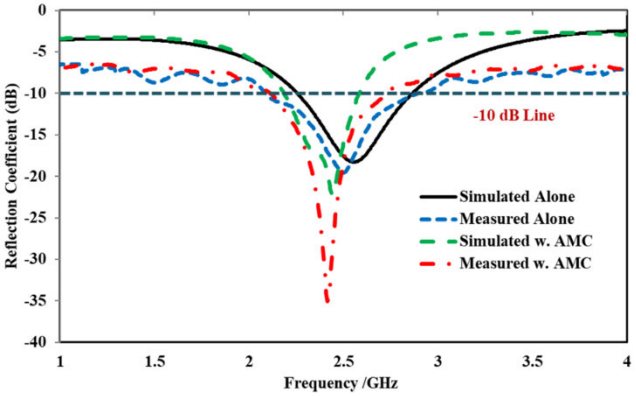

FIGURE 26. Simulated and measured reflection coefficient comparisons of antenna alone and AMC-integrated antenna mounted on human body arm at x = 0.05λ_o.

alone on a human body arm changed its center frequency, which shifted to higher frequencies owing to the human body's lossy properties and the electrical length shortening. In addition, the antenna resonated with a slightly wider bandwidth than in the off-body condition. Moreover, this trend was observed in the simulations.

Conversely, when the AMC-integrated antenna was kept in the same position as the human arm, a stable reflection coefficient (S_{11} < -36 dB) was observed compared with the antenna alone. Moreover, the impedance bandwidth was maintained similar to the off-body state, with a slight increase in width. The widening of the bandwidth in both cases was due to the degradation of the quality factor of the radiator element caused by lossy human body tissue [34].

The gain patterns of the antenna alone and the AMC-integrated antenna in both principal planes were measured by mounting both designs on the arms of the volunteers,

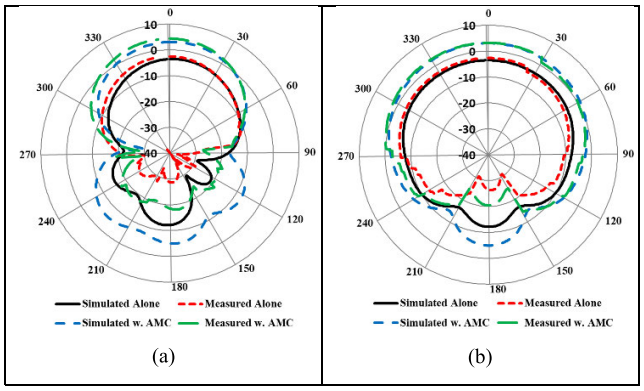

FIGURE 27. On- and Off-body simulated and measured far-field gain comparison of antenna alone and AMC-integrated antenna mounted on human body arm in (a) E-plane, and (b) H-plane.

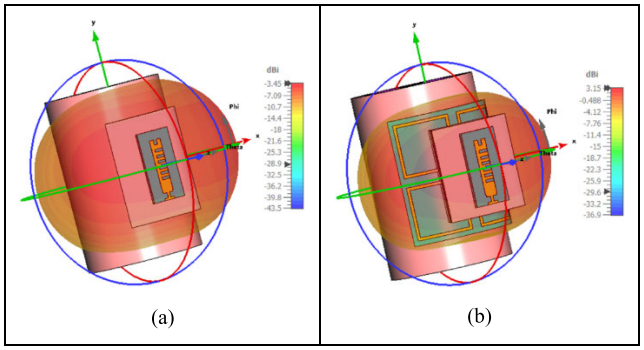

FIGURE 28. Perspective view of simulated 3D-gain pattern of proposed antenna mounted on arm tissue with radius of 40 mm (a) antenna alone (b) AMC-Integrated antenna.

as shown in Figs. 25 (d) and (e), respectively. The on-body measured results were compared with the simulated results obtained from a four-layer simplified body tissue arm model (Figs. 25 (b) and (c)) in both principal planes. The measured results revealed that the radiation pattern degraded when the antenna was tested close to the human arm. This degradation is due to the lossy properties of the arm tissues, reducing the peak gain and efficiency. However, when the AMC-integrated design was tested near the human arm, it exhibited stable performance at the resonant frequency (2.45 GHz), with an increase in peak gain and radiation efficiency. These results demonstrated the benefits of using the AMC surface as a ground plane.

For clarity, images of the simulated 3D gain patterns of the proposed designs placed near the arm tissue are also included (Fig. 28). Table 8 summarizes the simulated and measured performance comparisons between the antenna alone and the AMC-integrated antenna.

IV. SPECIFIC ABSORPTION RATE (SAR) ANALYSIS

The SAR of both the antenna alone and the AMC-integrated antenna must be evaluated to ensure the protection of human body tissue. The same flat body tissues (single, three, and four layers) and a cylindrical model mimicking the human

TABLE 8. On-body performance comparison of proposed designs mounted on human arm.

Parameters	Antenna Alone		AMC-Integrated	
	Simulated	Measured	Simulated	Measured
Frequency (GHz)	2.57	2.52	2.46	2.44
Gain (dBi)	-3.45	-2.59	3.15	4.11
Rad. Eff. (%)	14.08	15.76	69.71	67.22
-10 dB BW (MHz)	590	760	570	620

chest/back and arm presented in Section III were used for the analysis. An input power of 0.5 watts was used as a benchmark for evaluating the antenna alone and that integrated into the AMC. The proposed designs were assessed based on IEEE C95.1, using CST MWS to calculate the SAR value. The SAR values were compared using the FCC and ICNIRP standards, which set maximum values of 1.6 W/kg for every 1 g of tissue mass and 2 W/kg for every 10 g. The antenna was placed at a minimum distance of 7 mm from a human tissue phantom (chest/back and arm) to analyze the SAR. The results showed that the maximum SAR values observed were 19.3, 17.2, and 17.7 W/kg for 1 g of mass tissue and 9.49, 9.31, and 9.32 W/kg for 10 g of mass tissue, when the antenna was mounted on a single-, three-, and four-layer human body tissue in a flat condition at 2.45 GHz (see Fig. 29). These values are significantly higher than the safety thresholds and do not meet the safety requirements. However, when the AMC was incorporated, as shown in Fig. 27, a substantial reduction in the SAR value was observed at an input power of 0.5 W. The maximum value of the SAR was reduced from 19.3 to 0.434, 17.2 to 0.381, and 17.7 to 0.342 W/kg for any 1 g of mass tissue for the single-layer, three-layer, and four-layer models, respectively. Likewise, the SAR maximum value was reduced from 9.49 to 0.239, 9.31 to 0.215, and 9.32 to 0.196 W/kg for 10 g of mass tissue for single-, three-, and four-layer models, respectively.

Similarly, following the guidelines established by the FCC and ICNIRP, the antenna alone and the antenna with AMC integration were analyzed on a four-layer cylindrical arm model to determine the SAR value, as shown in Fig. 30. The maximum SAR values observed for the antenna alone were 13.9 W/kg for any 1 g of tissue mass and 7.51 W/kg for any 10 g. However, when the AMC was integrated into the antenna, a considerable decrease in the SAR value was observed. The SAR values decreased to 0.759 W/kg and 0.389 W/kg for 1 g and 10 g of tissue mass, respectively, which are considerably lower than the defined thresholds of 1.6 W/kg and 10 W/kg. Therefore, the AMC-integrated antenna meets both safety standards and is suitable for body-centric communications.

A performance comparison between the proposed AMC-integrated fabric antenna and state-of-the-art MMT-based antennas reported in the literature was conducted, and a summary of the results is presented in Table 9. The proposed AMC-integrated antenna exhibited superior performance in terms of the peak gain and impedance bandwidth compared with the antennas reported in [28], [37], [39], [40], and [42].

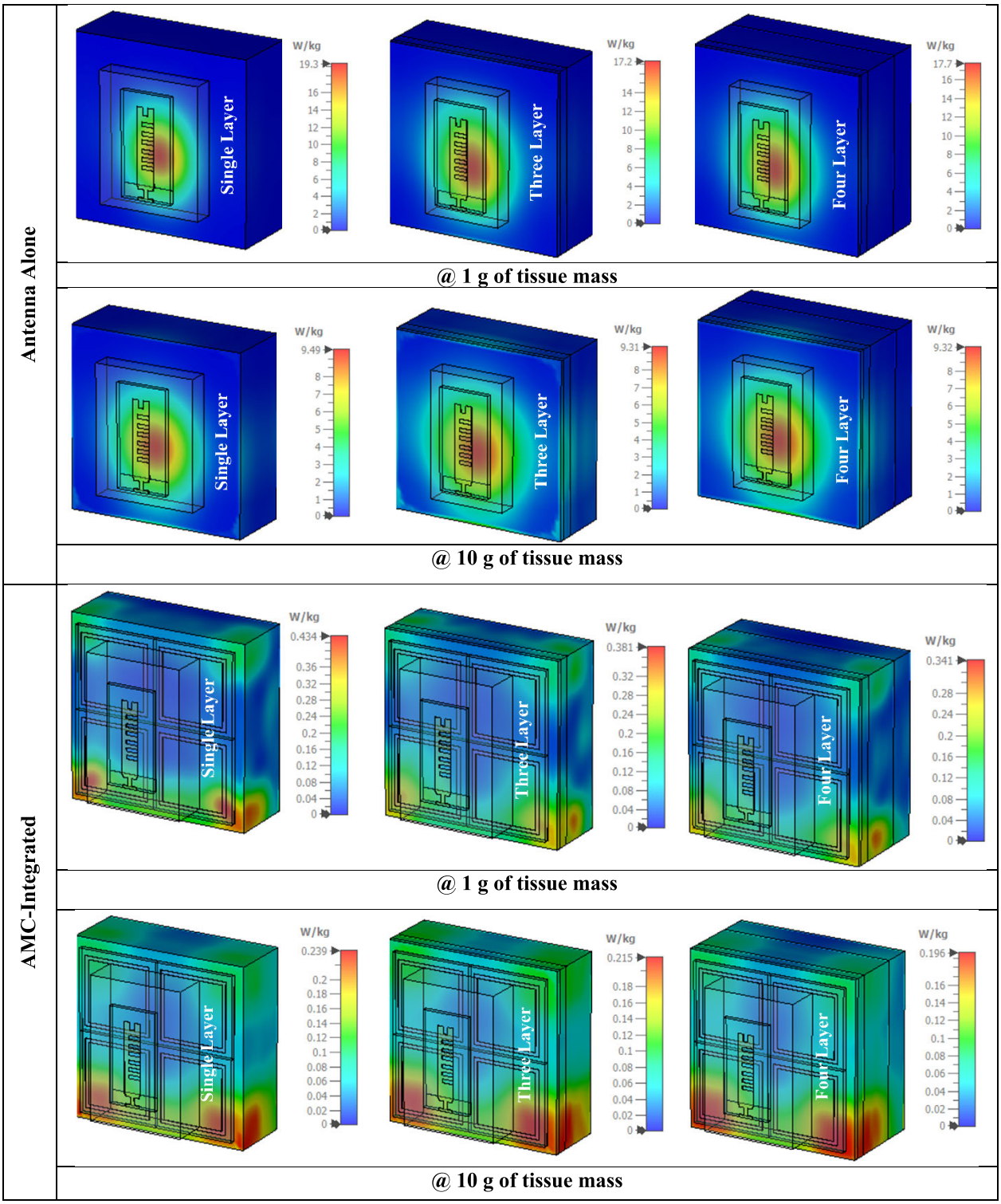

FIGURE 29. Simulated SAR distribution of antenna alone and AMC-integrated antenna on various tissue, considering 1 g and 10 g of human body tissue mass.

Despite using more lossy material, the proposed antenna provides better radiation efficiency in both on- and off-body conditions than the antennas in [28], [39], and [42]. The antennas reported in [36] and [38] provided a relatively higher gain than the proposed antenna; however, no information was provided regarding the on-body and off-body efficiencies. Although the antenna in [41] provides higher free-space efficiency owing to the less lossy material, the proposed design

TABLE 9. Summary of performance comparison of proposed AMC-integrated antenna with existing work at 2.45 GHz.

Ref.	Freq. (GHz)	Antenna Footprint (λ_o^3)	Gain (dBi) (FS)	BW (%)	Reflector/ Array	Efficiency (%)		SAR (W/Kg) @ Distance from body (λ_o)		Substrate/ Flexibility	Antenna Topology
						FS	OB	1 g	10 g		
[28]	2.45	0.81×0.81×0.036	2.50	--	AMC/ 4×4	<40	--	--	0.046@ 0.081	Felt/ Yes	CPW
[36]	2.40	1.08×1.08 ×0.025	7.93	1.38	EBG/ 3×3	--	--		0.07@ 0.024	Polyester Film/ Yes	Printed Yagi
[37]	2.45	1.22 ×1.22 ×0.016	--	5.08	EBG/ 3×3	--	--	--	0.02@ 0.008	Jeans/ Yes	Monopole
[38]	2.45	1.22 ×1.22 ×0.035	6.40	4.00	EBG/ 3×3	--	--	0.08@ 0.043	0.043@ 0.043	Felt/ Yes	Microstrip Patch
[39]	2.45	0.81×0.81×0.048	2.42	9.85	AMC/ 2×2	>40	--	--	0.072@ 0.122	Felt/ Yes	Monopole
[40]	2.45	1.01×1.01×0.040	2.45	16.32	AMC/ 4×4	95	66	0.33@ 0.04	0.166@ 0.04	Pellon & RO3003/ Flexible & Semi Flexible	CPW Monopole
[41]	2.45	0.62×0.62×0.021	6.58	6.40	EBG/ 3×3	98.5	38.84	0.022@ 0.025	0.0072@ 0.025	Rogers ULTRALAM 3850 & Felt/ Semi Flexible & Flexible	CPW Monopole
[42]	2.45	0.66×0.66×0.032	5.12	14.70	EBG/ 3×3	>60	--	0.55@ 0.048	0.23 0.048	Felt/ Yes	Monopole
This work	2.45	0.55×0.55×0.036	5.19	33.06	AMC/ 2×2	>83	>67	0.341 & 0.759 @0.008	0.196 & 0.389 @0.008	Felt/ Yes	Monopole

*λ_o is the free space wavelength computed at resonant frequency; **BW** represents the fractional bandwidth, **FS** represents Free Space, and **OB** represents On-body*

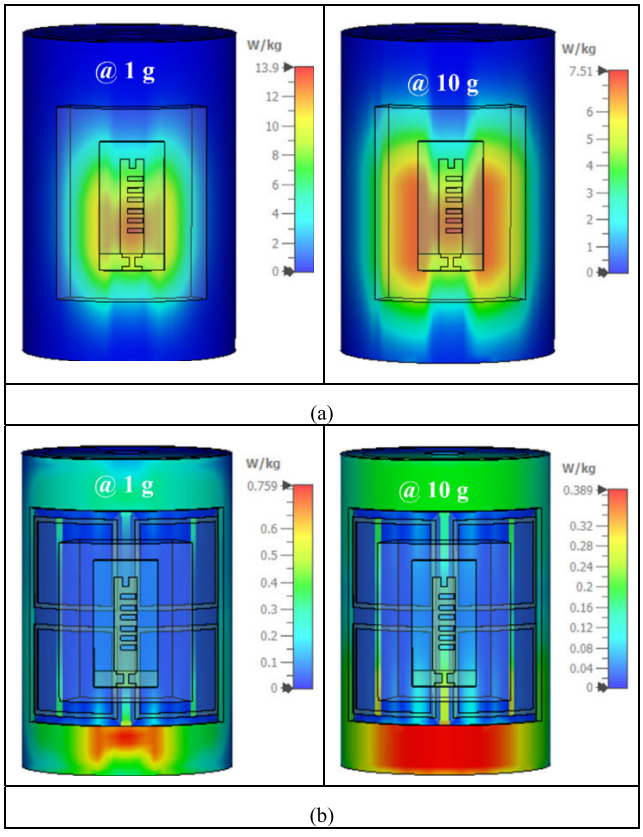

FIGURE 30. Simulated SAR distribution on four-layer human body arm with radius of 40 mm considering (a) antenna alone (b) AMC-Integrated antenna.

provides more bandwidth and better on-body efficiency. In contrast to most of the antennas shown in Table 9, the proposed AMC-integrated design offers a smaller footprint and a lower SAR value when accounting for both 1 and 10 g of tissue mass at a closer distance from human tissues. These characteristics make the proposed AMC integrated design suitable for body-centric communications.

V. CONCLUSION

In this study, a low-profile AMC-based fabric antenna for body-centric communication in the 2.45-GHz-centered ISM frequency range was designed, and its SAR analysis is presented. A 2 × 2 AMC array was incorporated into the proposed antenna to enhance the performance and reduce unwanted radiation when worn on the body. The antenna and AMC array were printed using a 0.17-mm thick superconductive Shieldit material with an estimated conductivity of 1.8510^5 S/m on a 2-mm thick flexible felt substrate with a relative permittivity of 1.3 and loss tangent of 0.044. The total size of the AMC-integrated antenna was $0.55\lambda_o \times 0.55\lambda_o \times 0.016\lambda_o$. The resonance frequency was preserved by integrating the AMC array, leading to considerable improvements in the peak gain and overall performance of both on- and off-bodies. To confirm the safety of the proposed antenna for body-centric communication, its SAR value was examined, and for the AMC integrated antenna, the value of SAR was found to be within the safety limits set by regulatory bodies, indicating its safety for human exposure. The simulated and tested results were compared, and they agreed well. The proposed design's flexibility, wearability, and low-profile characteristics make it suitable for wearable applications. The use of AMC structure was an effective method for enhancing the antenna's performance and decreasing SAR values. This study demonstrates the potential of AMC-based wearable antennas for a range of wireless applications, such as fitness monitoring, tracking, and healthcare.

Further studies should be conducted to improve the design of the antenna and examine its performance in real-world settings. In addition, the impact of different human body shapes and sizes on SAR can be investigated. Finally, to develop a complete wearable system, the integration of the antenna with other wearable technologies should be investigated.

ACKNOWLEDGMENT

(Usman Ali and Abdul Basir are co-first authors.)

REFERENCES

[1] A. Y. I. Ashyap, S. H. Dahlan, Z. Z. Abidin, M. R. Kamarudin, H. A. Majid, N. A. M. Alduais, M. H. Dahri, and S. A. Alhandi, "C-shaped antenna based artificial magnetic conductor structure for wearable IoT healthcare devices," *Wireless Netw.*, vol. 27, no. 7, pp. 4967–4985, Oct. 2021.

[2] S. Varma, S. Sharma, M. John, R. Bharadwaj, A. Dhawan, and S. K. Koul, "Design and performance analysis of compact wearable textile antennas for IoT and body-centric communication applications," *Int. J. Antennas Propag.*, vol. 2021, pp. 1–12, Aug. 2021.

[3] J.-F. Wu, C. Qiu, Y. Wang, R. Zhao, Z.-P. Cai, X.-G. Zhao, S.-S. He, F. Wang, Q. Wang, and J.-Q. Li, "Human limb motion detection with novel flexible capacitive angle sensor based on conductive textile," *Electronics*, vol. 7, no. 9, p. 192, Sep. 2018.

[4] F. Faisal, Y. Amin, Y. Cho, and H. Yoo, "Compact and flexible novel wideband flower-shaped CPW-fed antennas for high data wireless applications," *IEEE Trans. Antennas Propag.*, vol. 67, no. 6, pp. 4184–4188, Jun. 2019, doi: 10.1109/TAP.2019.2911195.

[5] A. Y. I. Ashyap, Z. Z. Abidin, S. H. Dahlan, H. A. Majid, and G. Saleh, "Metamaterial inspired fabric antenna for wearable applications," *Int. J. RF Microw. Comput.-Aided Eng.*, vol. 29, no. 3, Mar. 2019, Art. no. e21640.

[6] U. Ali, S. Ullah, B. Kamal, L. Matekovits, and A. Altaf, "Design, analysis and applications of wearable antennas: A review," *IEEE Access*, vol. 11, pp. 14458–14486, 2023.

[7] P. M. Potey and K. Tuckley, "Design of wearable textile antenna for low back radiation," *J. Electromagn. Waves Appl.*, vol. 34, no. 2, pp. 235–245, Jan. 2020.

[8] M. El Gharbi, R. Fernández-García, and I. Gil, "Embroidered wearable antenna-based sensor for real-time breath monitoring," *Measurement*, vol. 195, May 2022, Art. no. 111080.

[9] A. Ahmad, F. Faisal, S. Ullah, and D.-Y. Choi, "Design and SAR analysis of a dual band wearable antenna for WLAN applications," *Appl. Sci.*, vol. 12, no. 18, p. 9218, Sep. 2022.

[10] U. Ali, S. Ullah, M. Shafi, S. A. A. Shah, I. A. Shah, and J. A. Flint, "Design and comparative analysis of conventional and metamaterial-based textile antennas for wearable applications," *Int. J. Numer. Model., Electron. Netw., Devices Fields*, vol. 32, no. 6, p. 2567, Nov. 2019.

[11] A. Yadav, V. K. Singh, P. Yadav, A. K. Beliya, A. K. Bhoi, and P. Barsocchi, "Design of circularly polarized triple-band wearable textile antenna with safe low SAR for human health," *Electronics*, vol. 9, no. 9, p. 1366, Aug. 2020.

[12] O. M. Youssef, M. E. Atrash, and M. A. Abdalla, "A compact fully fabric I-shaped antenna supported with textile-based AMC for low SAR 2.45 GHz wearable applications," *Microw. Opt. Technol. Lett.*, vol. 65, no. 7, pp. 2021–2030, Jul. 2023.

[13] M. N. Shakib, M. Moghavvemi, and W. N. L. B. W. Mahadi, "Design of a tri-band off-body antenna for WBAN communication," *IEEE Antennas Wireless Propag. Lett.*, vol. 16, pp. 210–213, 2017.

[14] A. Michel, R. Colella, G. A. Casula, P. Nepa, L. Catarinucci, G. Montisci, G. Mazzarella, and G. Manara, "Design considerations on the placement of a wearable UHF-RFID PIFA on a compact ground plane," *IEEE Trans. Antennas Propag.*, vol. 66, no. 6, pp. 3142–3147, Jun. 2018.

[15] P. Mousavi, B. Miners, and O. Basir, "Wideband L-shaped circular polarized monopole slot antenna," *IEEE Antennas Wireless Propag. Lett.*, vol. 9, pp. 822–825, 2010.

[16] J. C. Bohorquez, H. A. F. Pedraza, I. C. H. Pinzon, J. A. Castiblanco, N. Pena, and H. F. Guarnizo, "Planar substrate integrated waveguide cavity-backed antenna," *IEEE Antennas Wireless Propag. Lett.*, vol. 8, pp. 1139–1142, 2009.

[17] R. Moro, S. Agneessens, M. Bozzi, and H. Rogier, "Wearable textile antenna in substrate integrated waveguide technology," *Electron. Lett.*, vol. 48, no. 16, pp. 985–987, Aug. 2012.

[18] P. J. Soh, G. A. E. Vandenbosch, S. L. Ooi, and N. H. M. Rais, "Design of a broadband all-textile slotted PIFA," *IEEE Trans. Antennas Propag.*, vol. 60, no. 1, pp. 379–384, Jan. 2012.

[19] A. Alomainy, Y. Hao, A. Owadally, C. G. Parini, Y. Nechayev, C. C. Constantinou, and P. S. Hall, "Statistical analysis and performance evaluation for on-body radio propagation with microstrip patch antennas," *IEEE Trans. Antennas Propag.*, vol. 55, no. 1, pp. 245–248, Jan. 2007.

[20] Y.-T. Hsiao, S.-C. Tuan, H.-T. Chou, and J.-S. Wang, "Applications of shielding techniques to enhance the antenna performance of mobile communications and reduce SAR induction in the human head," *Electromagnetics*, vol. 25, no. 4, pp. 343–361, May 2005.

[21] K. H. Chan, K. M. Chow, L. C. Fung, and S. W. Leung, "Effects of using conductive materials for SAR reduction in mobile phones," *Microw. Opt. Technol. Lett.*, vol. 44, no. 2, pp. 140–144, Jan. 2005.

[22] M. Haridim, "Use of rod reflectors for SAR reduction in human head," *IEEE Trans. Electromagn. Compat.*, vol. 58, no. 1, pp. 40–46, Feb. 2016.

[23] B. Kamal, U. Ali, J. Chen, and S. Ullah, "Applications of metamaterials and metasurfaces," in *Metamaterials—History, Current State, Applications, and Perspectives*. London, U.K.: IntechOpen, Nov. 2022.

[24] J. Lai, J. Wang, W. Sun, R. Zhao, and H. Zeng, "A low profile artificial magnetic conductor based tri-band antenna for wearable applications," *Microw. Opt. Technol. Lett.*, vol. 64, no. 1, pp. 123–129, Jan. 2022.

[25] A. Y. I. Ashyap, S. H. B. Dahlan, Z. Zainal Abidin, M. I. Abbasi, M. R. Kamarudin, H. A. Majid, M. H. Dahri, M. H. Jamaluddin, and A. Alomainy, "An overview of electromagnetic band-gap integrated wearable antennas," *IEEE Access*, vol. 8, pp. 7641–7658, 2020.

[26] K. Jairath, N. Singh, M. Shabaz, V. Jagota, and B. K. Singh, "Performance analysis of metamaterial-inspired structure loaded antennas for narrow range wireless communication," *Sci. Program.*, vol. 2022, pp. 1–17, May 2022.

[27] G.-P. Gao, B.-K. Zhang, J.-H. Dong, Z.-H. Dou, Z.-Q. Yu, and B. Hu, "A compact dual-mode pattern-reconfigurable wearable antenna for the 2.4-GHz WBAN application," *IEEE Trans. Antennas Propag.*, vol. 71, no. 2, pp. 1901–1906, Feb. 2023.

[28] S. Yan, P. J. Soh, and G. A. E. Vandenbosch, "Low-profile dual-band textile antenna with artificial magnetic conductor plane," *IEEE Trans. Antennas Propag.*, vol. 62, no. 12, pp. 6487–6490, Dec. 2014.

[29] M. Ur-Rehman, T. Kalsoom, N. A. Malik, G. A. Safdar, H. T. Chatha, N. Ramzan, and Q. H. Abbasi, "A wearable antenna for mmWave IoT applications," in *Proc. IEEE Int. Symp. Antennas Propag. USNC/URSI Nat. Radio Sci. Meeting*, Boston, MA, USA, Jul. 2018, pp. 1211–1212.

[30] K. Islam, A. Ahmed, and M. M. Khan, "Design evaluation of a millimeter-wave 60 GHz transparent antenna for body-centric communication in healthcare application," in *Proc. Int. Conf. Adv. Electr. Electron. Eng. (ICAEEE)*, Feb. 2022, pp. 1–5.

[31] J. Pourahmadazar and T. A. Denidni, "60 GHz antenna array for millimeter-wave wireless sensor devices using silver nanoparticles ink mounted on a flexible polymer substrate," *Microw. Opt. Technol. Lett.*, vol. 59, no. 11, pp. 2830–2835, Nov. 2017.

[32] R. Bharadwaj, S. Swaisaenyakorn, C. G. Parini, J. C. Batchelor, and A. Alomainy, "Impulse radio ultra-wideband communications for localization and tracking of human body and limbs movement for healthcare applications," *IEEE Trans. Antennas Propag.*, vol. 65, no. 12, pp. 7298–7309, Dec. 2017.

[33] A. Yadav, V. K. Singh, A. K. Bhoi, G. Marques, B. Garcia-Zapirain, and I. D. L. T. Díez, "Wireless body area networks: UWB wearable textile antenna for telemedicine and mobile health systems," *Micromachines*, vol. 11, no. 6, p. 558, May 2020.

[34] A. Y. I. Ashyap, Z. Z. Abidin, S. H. Dahlan, H. A. Majid, M. R. Kamarudin, A. Alomainy, R. A. Abd-Alhameed, J. S. Kosha, and J. M. Noras, "Highly efficient wearable CPW antenna enabled by EBG-FSS structure for medical body area network applications," *IEEE Access*, vol. 6, pp. 77529–77541, 2018.

[35] M. S. Alam, M. T. Islam, and N. Misran, "A novel compact split ring slotted electromagnetic bandgap structure for microstrip patch antenna performance enhancement," *Prog. Electromagn. Res.*, vol. 130, pp. 389–409, 2012.

[36] B. S. Abirami and E. F. Sundarsingh, "EBG-backed flexible printed Yagi–Uda antenna for on-body communication," *IEEE Trans. Antennas Propag.*, vol. 65, no. 7, pp. 3762–3765, Jul. 2017.

[37] S. Velan, E. F. Sundarsingh, M. Kanagasabai, A. K. Sarma, C. Raviteja, R. Sivasamy, and J. K. Pakkathillam, "Dual-band EBG integrated monopole antenna deploying fractal geometry for wearable applications," *IEEE Antennas Wireless Propag. Lett.*, vol. 14, pp. 249–252, 2015.
[38] S. Zhu and R. Langley, "Dual-band wearable textile antenna on an EBG substrate," *IEEE Trans. Antennas Propag.*, vol. 57, no. 4, pp. 926–935, Apr. 2009.
[39] H. Lago, P. J. Soh, M. F. Jamlos, N. Shohaimi, S. Yan, and G. A. E. Vandenbosch, "Textile antenna integrated with compact AMC and parasitic elements for WLAN/WBAN applications," *Appl. Phys. A, Solids Surf.*, vol. 122, no. 12, pp. 1–6, Dec. 2016.
[40] A. Alemaryeen and S. Noghanian, "Crumpling effects and specific absorption rates of flexible AMC integrated antennas," *IET Microw., Antennas Propag.*, vol. 12, no. 4, pp. 627–635, Mar. 2018.
[41] M. El Atrash, O. F. Abdalgalil, I. S. Mahmoud, M. A. Abdalla, and S. R. Zahran, "Wearable high gain low SAR antenna loaded with backed all-textile EBG for WBAN applications," *IET Microw., Antennas Propag.*, vol. 14, no. 8, pp. 791–799, Jul. 2020.
[42] G.-P. Gao, B. Hu, S.-F. Wang, and C. Yang, "Wearable circular ring slot antenna with EBG structure for wireless body area network," *IEEE Antennas Wireless Propag. Lett.*, vol. 17, no. 3, pp. 434–437, Mar. 2018.

USMAN ALI received the B.Sc. and M.Sc. degrees in telecommunication engineering from the University of Engineering and Technology (UET), Peshawar, Pakistan, in 2012 and 2017, respectively, where he is currently pursuing the Ph.D. degree in telecommunication engineering. He is a Lecturer with the Department of Telecommunication Engineering, UET Mardan, Pakistan. His research interests include wearable antennas, SAR analysis, 5G antennas, millimeters wave antennas, reconfigurable antennas, metamaterials, and electromagnetic band-gap structures.

SADIQ ULLAH (Senior Member, IEEE) received the B.Sc. degree in electrical engineering from the University of Engineering and Technology, Peshawar, Peshawar, Pakistan, the M.Sc. degree in electrical engineering from the University of Engineering and Technology, Taxila, Pakistan, and the Ph.D. degree for his research in the field of design and measurement of metamaterial-based antennas, in 2010. In 2007, he joined the Department of Electronic and Electrical Engineering, Loughborough University, U.K. He was an Assistant Manager (Electronics) in a public sector research and development organization in Islamabad, where his main responsibilities were hardware, software co-design, designing and testing of high precession electronics, and test equipment. He was a Research Associate with Loughborough University, researching the propagation effects of rain, snow, ice, fog, and forest in millimeter wave bands. He is currently a Professor and the Head of the Telecommunication Engineering Department, University of Engineering and Technology, Mardan, Mardan, Pakistan. His research has been published in international conferences and peer-reviewed journals. His research interests include the design and measurement of metasurfaces, metamaterial-based antennas, 5G MIMO antennas, multiband/wideband antennas, SAR, and wearable antennas.

ABDUL BASIR (Member, IEEE) was born in Khyber Pakhtunkhwa, Pakistan, in 1989. He received the B.Sc. degree in telecommunication engineering from the University of Engineering and Technology, Peshawar, Pakistan, in 2015, and the Ph.D. degree in electronic engineering from Hanyang University, Seoul, South Korea, in 2021. He is currently a Postdoctoral Researcher with Hanyang University. His research interests include implantable antennas and systems, biomedical circuits, wearable antennas, MIMO communication, metamaterial, dielectric resonator antennas, reconfigurable antennas, long-range wireless power transfer, and wireless charging of biomedical implants. He received the Silver Prize for the Best Student Paper Award from Student Paper Contests 2018 and 2019, IEEE Seoul Section. His collaborated paper received the Best Paper Award by the IEEE AP/MTT/EMC Joint Chapter Malaysia, in 2019. In addition, he received the Third Prize for the Best Student Paper Completion 2018 by the Korea Communications Agency (KCA) and the Korean Institute of Electromagnetic Engineering and Science (KIEES).

BABAR KAMAL received the B.Sc. degree in electronics engineering from BUITEMS, Quetta, Pakistan, the M.Sc. degree in telecommunication engineering from the University of Engineering and Technology, Peshawar, Pakistan, and the Ph.D. degree in information and communication engineering from Northwestern Polytechnical University (NWPU), China. He is currently a Postdoctoral Fellow with the Center of Intelligent Acoustics and Immersive Communication, School of Marine Science and Technology, NWPU. His research interests include metasurfaces, metamaterials, wearable antennas, multiband and wideband antennas, polarization control devices, and absorbers.

LADISLAU MATEKOVITS (Senior Member, IEEE) received the degree in electronic engineering from Institutul Politehnic din Bucureşti, Bucureşti, Romania, in 1992, and the Ph.D. (Dottorato di Ricerca) degree in electronic engineering from Politecnico di Torino, Torino, Italy, in 1995.

Since 1995, he has been with the Department of Electronics and Telecommunications, Politecnico di Torino, first with a postdoctoral fellowship, and then as a Research Assistant. He joined the Department of Electronics and Telecommunications, Politecnico di Torino, as an Assistant Professor, in 2002, and was appointed as a Senior Assistant Professor, in 2005, and as an Associate Professor, in 2014. In late 2005, he was a Visiting Scientist with the Antennas and Scattering Department, FGAN-FHR (now Fraunhofer Institute), Wachtberg, Germany. In July 2009, he joined Macquarie University, Sydney, NSW, Australia, as a Marie Curie Fellow, for two years, where he also held a visiting academic position, in 2013. In 2014, he has been appointed as an Honorary Fellow. In February 2017, he was a Full Professor in Italy. Since 2020, he has been an Honorary Professor with the Polytechnic University of Timisoara, Romania, and an Associate of the Italian National Research Council. He has been invited to serve as a Research Grant Assessor for government funding calls (Romania, Italy, Croatia, Kazakhstan, and Iceland) and as an international expert in Ph.D. thesis evaluation by several universities from Australia, India, Pakistan, and Spain. He has published more than 400 articles, including more than 125 journal contributions, and delivered seminars on these topics all around the world: Europe, USA (AFRL/MIT-Boston), Australia, China, and Russia. His main research interests include numerical analysis of printed antennas and in particular development of new, numerically efficient full-wave techniques to analyze large arrays, and active and passive metamaterials for cloaking applications. Material parameter retrieval of these structures by inverse methods and different optimization techniques has also been considered. In the last years, bio-electromagnetic aspects have also been contemplated, such as example design of implantable antennas or the development of nano-antennas for example for drug delivery applications.

Prof. Matekovits has been a member of the Organizing Committee of the International Conference on Electromagnetics in Advanced Applications (ICEAA), since 2010. He has been appointed as a member of the National Council for the Attestation of University Degrees, Diplomas and Certificates (CNATDCU), Romania, during 2020–2024. He is a member of the International Advisory Committee and the technical program committee of several conferences. He was a recipient of various awards in international conferences, including the 1998 URSI Young Scientist Award (Thessaloniki, Greece), the Barzilai Award 1998 (Young Scientist Award, granted every two years by the Italian National Electromagnetic Group), and the Best AP2000 Oral Paper on Antennas, ESA-EUREL Millennium Conference on Antennas and Propagation (Davos, Switzerland). He was a recipient of the Motohisa Kanda Award, in 2018, for the most cited paper of the IEEE TRANSACTIONS ON ELECTROMAGNETIC COMPATIBILITY in the past five years. He received the 2019 American Romanian Academy of Arts and Sciences (ARA) Medal of Excellence in Science and the Ad Astra Award in 2020, a Senior Researcher for Excellence in Research, the Outstanding Associate Editor Award for the IEEE ANTENNAS AND WIRELESS PROPAGATION LETTERS, in 2020, and one of the scientists with the highest level of scientific productivity (the top 2% in the world) prepared by Stanford University researchers, in 2022. He has been an Assistant Chairperson and the Publication Chairperson of the European Microwave Week 2002, Milan, Italy, and the General Chair of the 11th International Conference on Body Area Networks (BodyNets) 2016. He serves as an Associate Editor for the IEEE TRANSACTIONS ON ANTENNAS AND PROPAGATION, IEEE ACCESS, IEEE ANTENNAS AND WIRELESS PROPAGATION LETTERS, and *IET MAP*, and a reviewer for different journals.

HYOUNGSUK YOO (Senior Member, IEEE) received the B.Sc. degree in electrical engineering from Kyungpook National University, Daegu, South Korea, in 2003, and the M.Sc. and Ph.D. degrees in electrical engineering from the University of Minnesota, Minneapolis, MN, USA, in 2006 and 2009, respectively. In 2009, he joined the Center for Magnetic Resonance Research, University of Minnesota, as a Postdoctoral Associate. In 2010, he joined Cardiac Rhythm Disease Management, Medtronic, MN, USA, as a Senior EM/MRI Scientist. From 2011 to 2018, he was an Associate Professor with the Department of Biomedical Engineering, School of Electrical Engineering, University of Ulsan, Ulsan, South Korea. He has been the CEO of E2MR, Seoul, South Korea, a startup company, since 2017. Since 2018, he has been a Full Professor with the Department of Biomedical Engineering and the Department of Electronic Engineering, Hanyang University, Seoul. His current research interests include electromagnetic theory, numerical methods in electromagnetics, metamaterials, antennas, implantable devices, and magnetic resonance imaging in high-magnetic-field systems. He received the Third Prize for the Best Student Paper from the 2010 IEEE Microwave Theory and Techniques Society International Microwave Symposium.

Open Access funding provided by 'Politecnico di Torino' within the CRUI CARE Agreement